Geophysical Prospecting EAGE EUROPEAN ASSOCIATION OF GEOSCIENTISTS & ENGINEERS

Geophysical Prospecting, 2012, **60**, 1114–1132 doi: 10.1111/j.1365-2478.2011.01051.x

A hybrid absorbing boundary condition for elastic staggered-grid modelling

Yang Liu[1] and Mrinal K. Sen[2]

[1]*State Key Laboratory of Petroleum Resources and Prospecting (China University of Petroleum, Beijing), Beijing, China*
[2]*The Institute for Geophysics, John A. and Katherine G. Jackson School of Geosciences, The University of Texas at Austin, 10100 Burnet Road, R2200 Austin, TX 78758*

Received November 2010, revision accepted October 2011

ABSTRACT

We recently proposed an efficient hybrid scheme to absorb boundary reflections for acoustic wave modelling that could attain nearly perfect absorptions. This scheme uses weighted averaging of wavefields in a transition area, between the inner area and the model boundaries. In this paper we report on the extension of this scheme to 2D elastic wave modelling with displacement-stress formulations on staggered grids using explicit finite-difference, pseudo-implicit finite-difference and pseudo-spectral methods. Numerical modelling results of elastic wave equations with hybrid absorbing boundary conditions show great improvement for modelling stability and significant absorption for boundary reflections, compared with the conventional Higdon absorbing boundary conditions, demonstrating the effectiveness of this scheme for elastic wave modelling. The modelling results also show that the hybrid scheme works well in 2D rotated staggered-grid modelling for isotropic medium, 2D staggered-grid modelling for vertically transversely isotropic medium and 2D rotated staggered-grid modelling for tilted transversely isotropic medium.

Keywords: Absorbing boundary condition, Elastic wave, Staggered-grid, Explicit finite difference, Pseudo-implicit finite difference.

INTRODUCTION

Due to the finite computational domain, one of the persistent problems in the numerical solution of wave equations (WEs) is the artificial reflections from model boundaries. Three different approaches of absorbing boundary conditions (ABCs) to address this problem have been proposed in the literature. The first kind is a prediction-based method. The boundary wavefield values are usually predicted by some approximations such as one-way wave equations (OWWEs), field extrapolation, etc (e.g., Engquist and Majda 1977; Reynolds 1978; Liao *et al.* 1984; Higdon 1991). Since it is difficult to predict the boundary wavefield values very accurately in most cases, boundary reflections are still strong compared with the amplitudes of reflected waves from the reflectors in a model and relatively few researchers (e.g., Stacey 1988, 2003; Zhou and McMechan 2000; Heidari and Guddati 2006) have studied this method recently. The second is an attenuation-based method. Usually an exponential function is used to attenuate the wavefield within a pre-defined damping area near the boundary (e.g., Cerjan *et al.* 1985; Kosloff and Kosloff 1986; Sochacki *et al.* 1987). However, it is generally relatively difficult to design a proper attenuation function to perfectly absorb boundary reflections and thus very few developments have been reported in recent years (e.g., Sarma, Mallick

Email: wliuyang@vip.sina.com, mrinal@ig.utexas.edu

© 2012 European Association of Geoscientists & Engineers

and Gadhinglajkar 1998; Tian *et al*. 2008). The third is the perfectly matched layer (PML) method. In this method, the computational domain is wrapped by an absorbing material with appropriate decay factors designed to nearly perfectly absorb the outgoing waves (Bérenger 1994). Many developments have been reported for seismic modelling (e.g., Zeng, He and Liu 2001; Festa and Nielsen 2003; Wang and Tang 2003; Komatitsch and Tromp 2003; Hu, Abubakar and Habashy 2007; Gao and Zhang 2008) using this approach. The PML method is essentially a kind of attenuation-based method. Of these three methods, the prediction-based method has the least computational expense and it moderately absorbs boundary reflections. The attenuation-based method has moderate computational expense but performs the worst amongst the three. The PML method is the most expensive computationally but generally obtains the best absorption.

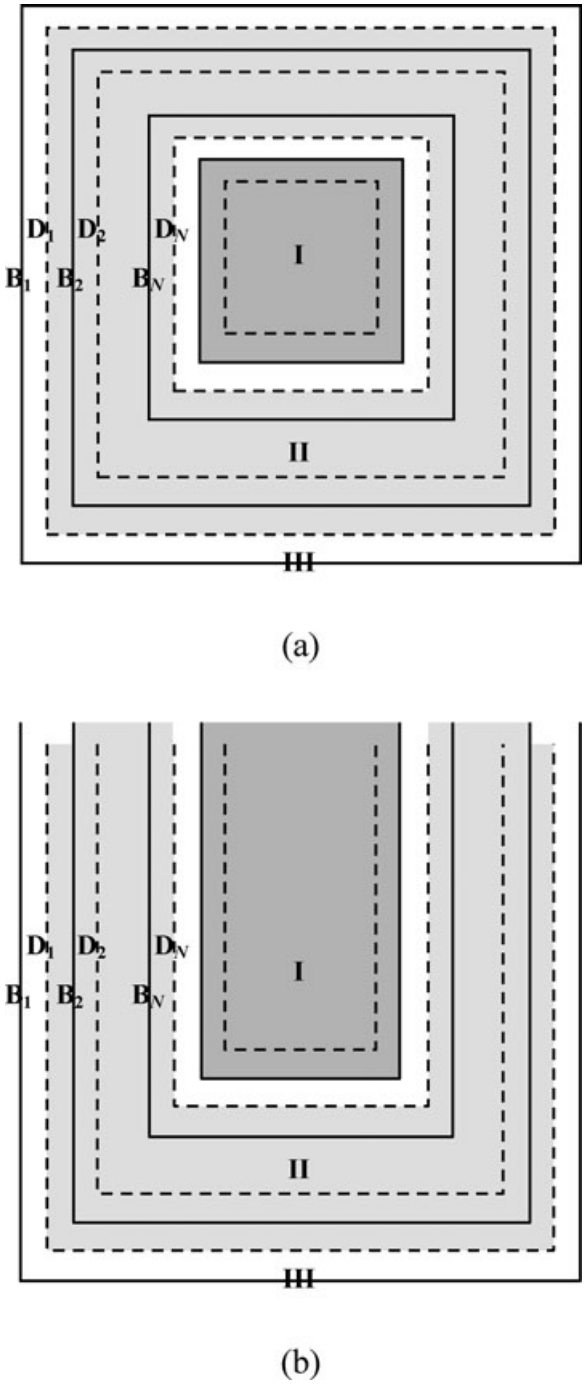

Figure 1. Illustration of hybrid absorbing boundary conditions for elastic staggered-grid modelling (a) without and (b) with free surface respectively. u_x is on grids of a solid frame and u_z is on grids of a dash frame.

Liu and Sen (2010a) analysed the prediction of a OWWEs based scheme. In this scheme, wavefields at the boundary grid points are calculated by a OWWE and those at the non-boundary grid points are determined by elastodynamic equations (e.g., Clayton and Engquist 1977). When the waves propagate from the non-boundary area to the boundary, a sharp variation occurs between the wavefields at the non-boundary and boundary grids since they are determined by different forms of the elastodynamic equation and different FD stencils. Therefore, there always exist some residual edge reflections. To decrease the sharp variation in the wavefield between non-boundary and boundary grids, Liu and Sen (2010a) proposed a new hybrid scheme, based on a weighted strategy for predicted and modelled wavefields in a transition area, for absorbing edge reflections, which has the advantages of small memory, small computation time and significant absorption. Liu and Sen (2010b) reported on the initial implementation of this scheme for elastic wave modelling with staggered-grid finite difference (FD). In this paper, we develop this scheme further for elastic wave modelling on staggered grids.

The structure of this paper is as follows. First, we introduce elastodynamic equations in displacement-stress formulations and their numerical modelling schemes on staggered grids. Then, we give the one-way wave equations and difference approximations. Hybrid absorption boundary conditions for elastic staggered-grid modelling are developed. In the examples section, we perform staggered-grid modelling on a homogeneous elastic model by the explicit finite-difference method (FDM), pseudo-implicit FDM and pseudo-spectral method to examine the effectiveness of the hybrid ABCs. We also perform modelling on an elastic model with high v_p/v_s and the Marmousi elastic model. In the discussion section, we develop the hybrid ABCs for rotated staggered-grid modelling in isotropic medium, staggered-grid modelling in vertically transversely isotropic (VTI) medium and rotated staggered-grid modelling in tilted transversely isotropic (TTI) medium.

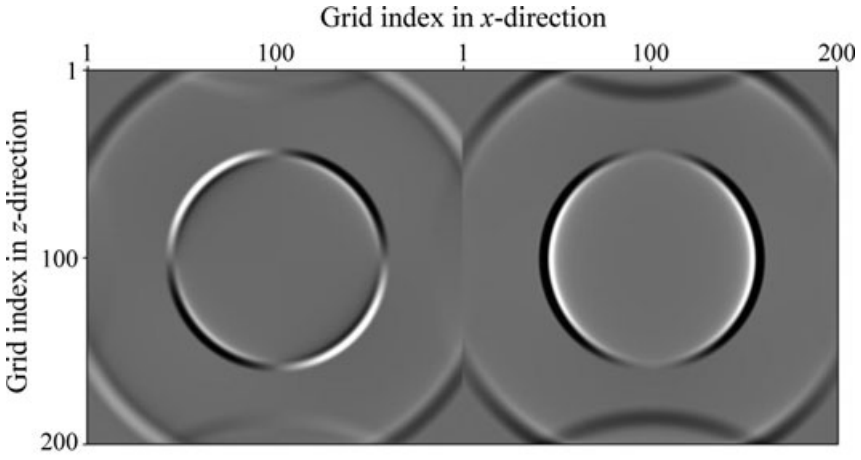

(a) $t = 400$ ms, hybrid ABCs, $N = 1$ (Higdon ABCs)

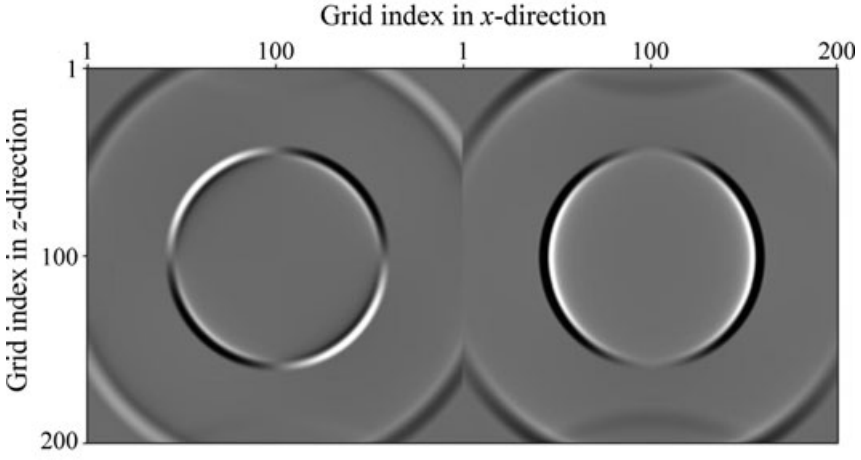

(b) $t = 400$ ms, hybrid ABCs, $N = 2$

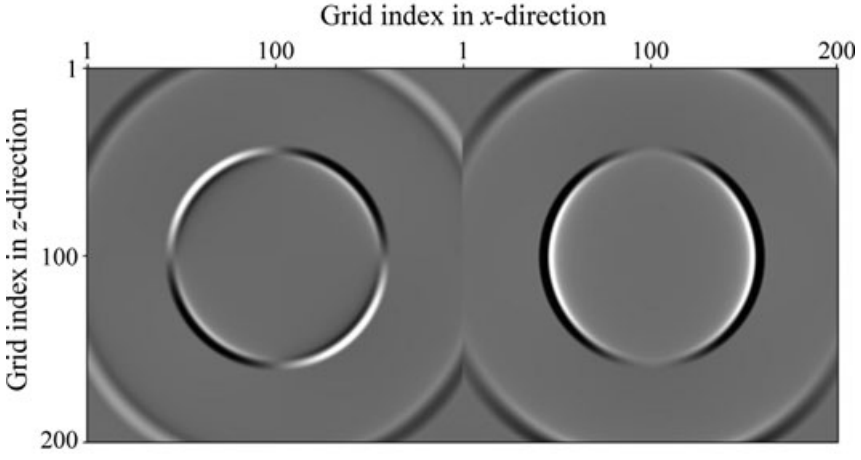

(c) $t = 400$ ms, hybrid ABCs, $N = 10$

Figure 2. Snapshots computed by 20th-order explicit staggered-grid FD modelling for a 2D homogeneous elastic model with hybrid ABCs. Each figure includes 2 panels with x- and z-components from left to right. Wavefields of grids used for ABCs are shown in all the figures.

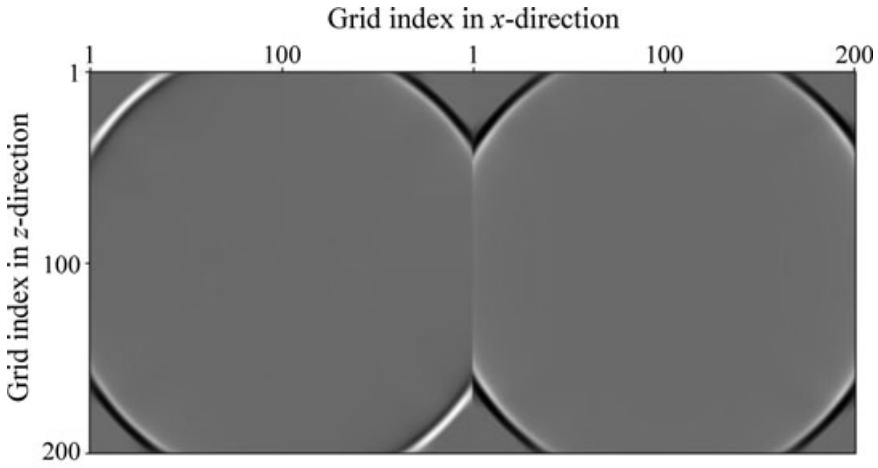

(d) $t = 800$ ms, hybrid ABCs, $N = 10$

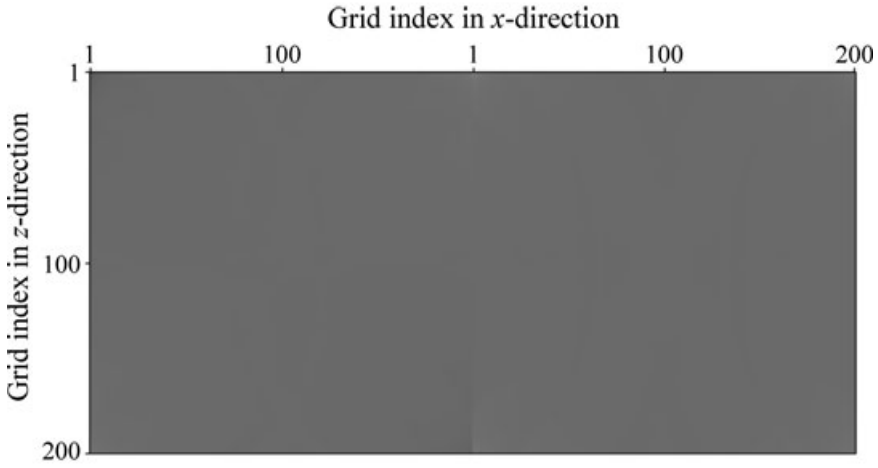

(e) $t = 1000$ ms, hybrid ABCs, $N = 10$

Figure 2. continued.

ELASTODYNAMIC EQUATIONS AND THEIR NUMERICAL MODELLING SCHEMES ON STAGGERED GRIDS

The displacement-stress relations of ealstodynamic equations in isotropic elastic medium are given by (e.g., Virieux 1986; Luo and Schuster 1990)

$$\rho \frac{\partial^2 u_x}{\partial t^2} = \frac{\partial \tau_{xx}}{\partial x} + \frac{\partial \tau_{xz}}{\partial z}, \tag{1a}$$

$$\rho \frac{\partial^2 u_z}{\partial t^2} = \frac{\partial \tau_{xz}}{\partial x} + \frac{\partial \tau_{zz}}{\partial z}, \tag{1b}$$

$$\tau_{xx} = (\lambda + 2\mu)\frac{\partial u_x}{\partial x} + \lambda \frac{\partial u_z}{\partial z}, \tag{1c}$$

$$\tau_{zz} = \lambda \frac{\partial u_x}{\partial x} + (\lambda + 2\mu)\frac{\partial u_z}{\partial z}, \tag{1d}$$

$$\tau_{xz} = \mu \left(\frac{\partial u_z}{\partial x} + \frac{\partial u_x}{\partial z} \right), \tag{1e}$$

where, (u_x, u_z) is the displacement vector, $(\tau_{xx}, \tau_{zz}, \tau_{xz})$ is a vector containing three components of stress, $\lambda(x, z)$ and $\mu(x, z)$ are Lame coefficients and $\rho(x, z)$ is the density.

The staggered-grid FD scheme (e.g., Virieux 1986; Luo and Schuster 1990; Liu and Sen 2009) is used to numerically solve elastic wave equations (1a)–(1e). Using a second-order explicit temporal FDM (FD method), equations (1a) and (1b) become

$$u_x(i,\,j,\,k+1) = 2u_x(i,\,j,\,k) - u_x(i,\,j,\,k-1) + \frac{(\Delta t)^2}{\rho}\left(\frac{\partial \tau_{xx}}{\partial x} + \frac{\partial \tau_{xz}}{\partial z}\right), \tag{2a}$$

$$u_z(i,\,j,\,k+1) = 2u_z(i,\,j,\,k) - u_z(i,\,j,\,k-1) + \frac{(\Delta t)^2}{\rho}\left(\frac{\partial \tau_{xz}}{\partial x} + \frac{\partial \tau_{zz}}{\partial z}\right), \tag{2b}$$

where, $(i,\,j,\,k)$ represents $(ih,\,jh,\,k\tau)$, h is grid size and Δt is time step.

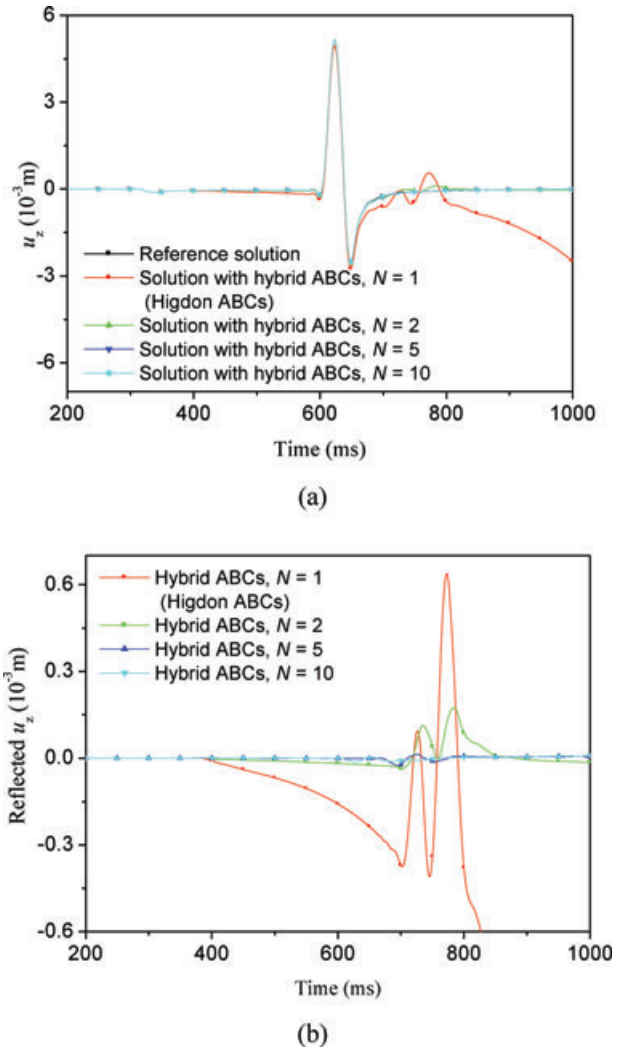

Figure 3. The received u_z at $(x,\,z)$ = (100 m, 900 m) and the artificially reflected wave caused by Higdon ABCs and hybrids ABCs. (a) Reference solution u_z, the solution with Higdon ABCs and the solution with hybrid ABCs. (b) The reflected wave u_z, i.e., the difference between the reference solution and the solution with Higdon ABCs or hybrid ABCs. All the parameters are the same as those in Fig. 2. The reference solution is calculated by extending the model boundaries.

There are several methods to calculate the spatial derivatives in equations (1a)–(1e) on staggered grids. Here, we use three methods, that is, explicit FDM (e.g., Kindelan, Kamel and Sguazzero 1990; Liu and Sen 2009), pseudo-implicit FDM (Liu and Sen 2009) and pseudo-spectral methods (e.g., Kosloff and Baysal 1982; Fornberg 1987).

In all the following modelling examples, we adopt the mirror-image symmetry boundary condition in calculating spatial derivatives for both explicit and pseudo-implicit FDMs to maintain $(2M)$th-order and $(2M+2)$th-order accuracy respectively near the boundaries. For the free surface, the mirror-image inverse symmetry boundary condition is used instead (e.g., Liu and Sen 2010a).

ONE-WAY WAVE EQUATIONS AND DIFFERENCE APPROXIMATIONS

We adopt the new hybrid scheme developed by Liu and Sen (2010a) to absorb reflections from the model boundaries in numerical solutions of elastodynamic equations. One of the key problems with this scheme is to choose the appropriate OWWEs. There are several OWWEs for elastic waves. The first-order OWWEs (e.g., Reynolds 1978) give significant absorption for outgoing plane waves travelling at certain velocities and/or angles of incidence but strong boundary reflections usually exist at other velocities and/or angles of incidence. We test these first-order OWWEs for hybrid ABCs

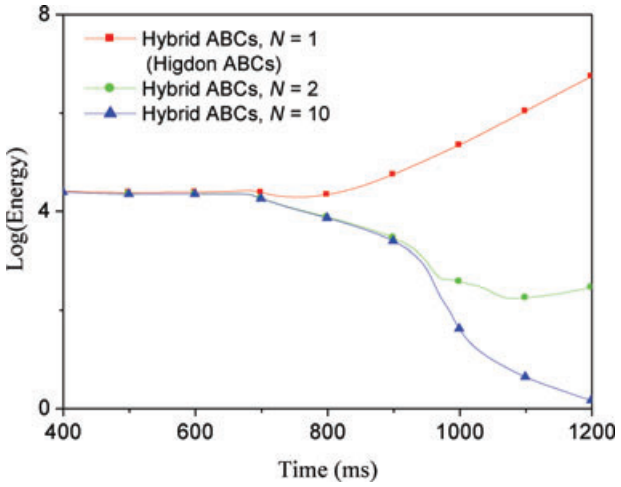

Figure 4. Variation of energy in the inner area with the modelling recursion time for the 2D homogeneous elastic model used in Fig. 2. The inner area is fixed as 2000 m × 2000 m and 20th-order explicit staggered-grid FD modelling with hybrid ABCs is used.

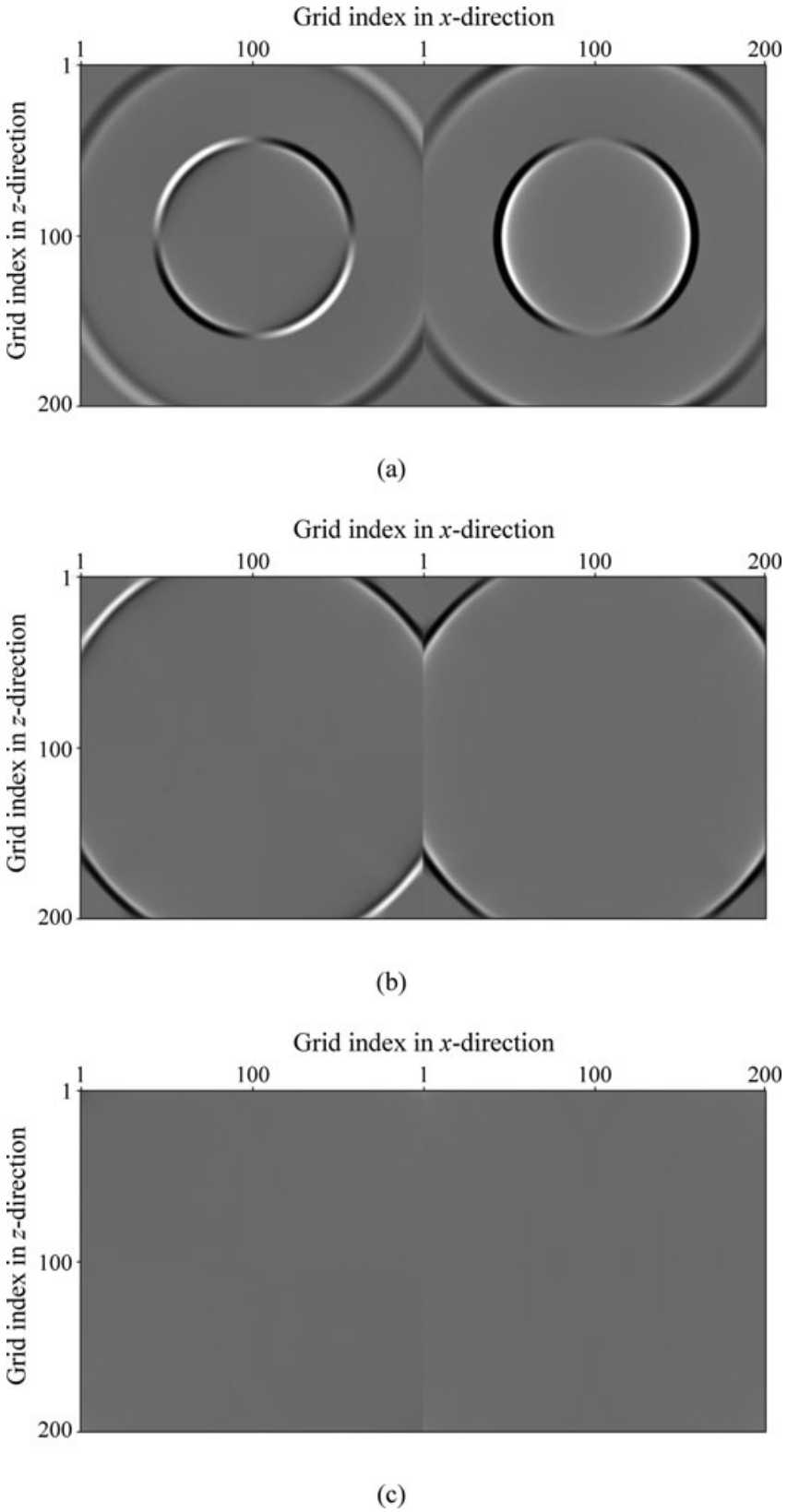

Figure 5. Snapshots computed by 12th-order pseudo-implicit staggered-grid FD modelling for a 2D homogeneous elastic model with hybrid ABCs ($N = 10$). (a) $t =$ 400 ms, (b) $t = 800$ ms, (c) $t = 1000$ ms. Each figure includes 2 panels with x- and z-components from left to right. Wavefields of grids used for ABCs are shown in all the figures.

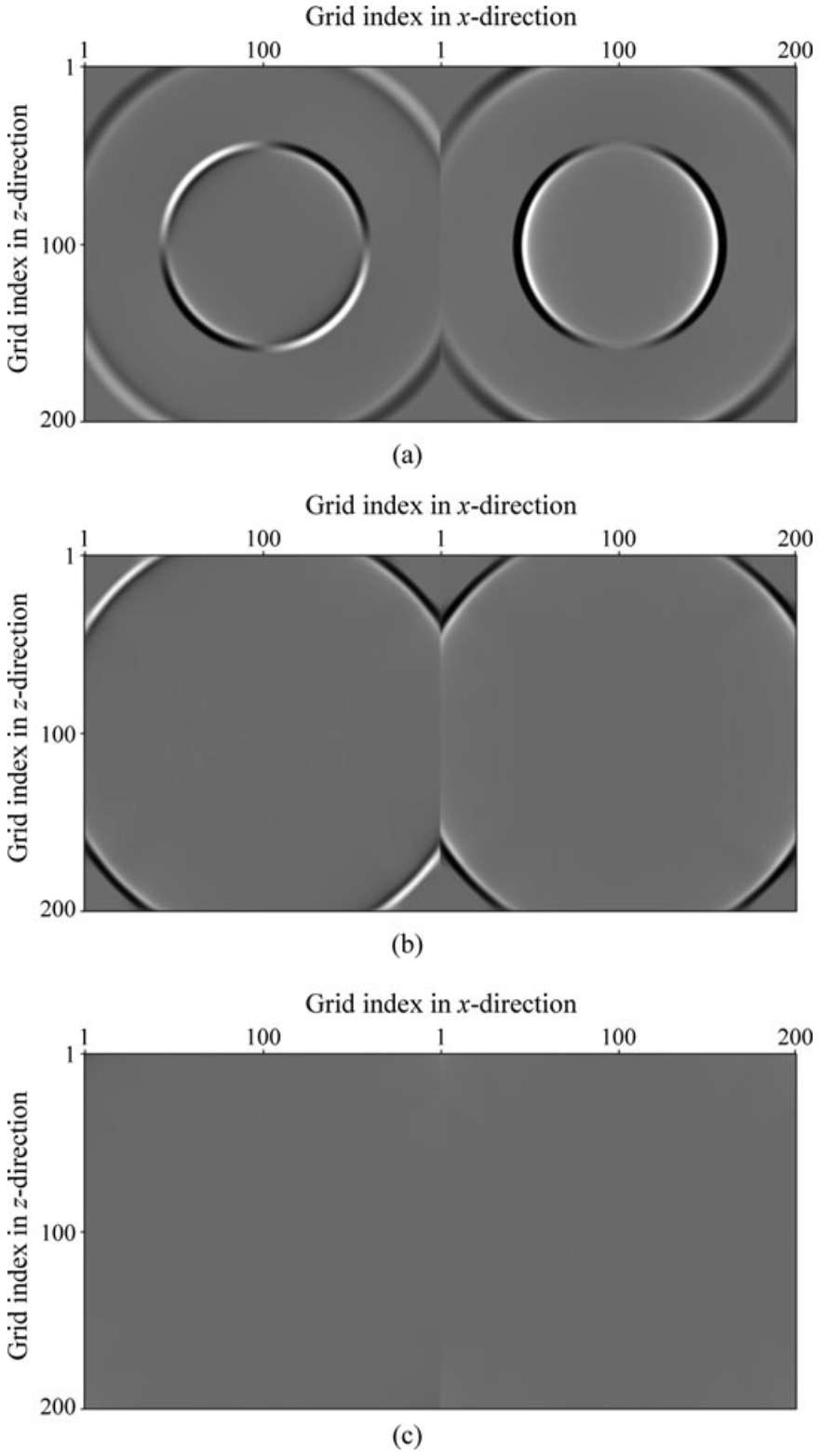

Figure 6. Snapshots computed by staggered-grid pseudo-spectral modelling for a 2D homogeneous elastic model with hybrid ABCs ($N = 10$). (a) $t = 400$ ms, (b) $t = 800$ ms, (c) $t = 1000$ ms. Each figure includes 2 panels with x- and z-components from left to right. Wavefields of grids used for ABCs are shown in all the figures.

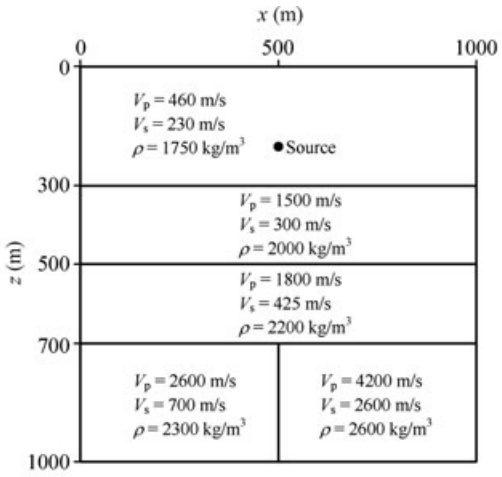

(a) Model parameters

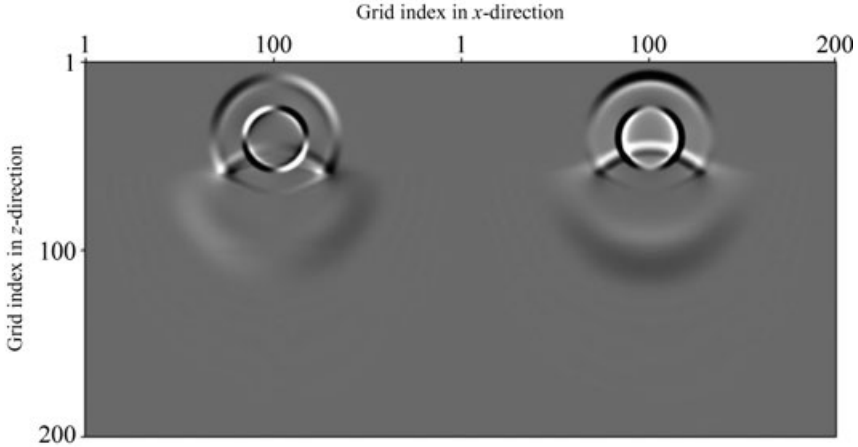

(b) Snapshot at 400 ms

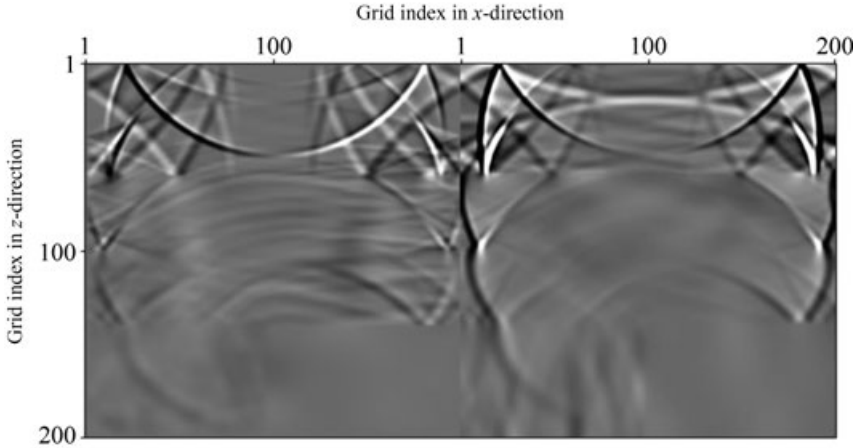

(c) Snapshot at 2000 ms without ABCs

Figure 7. Snapshots and seismograms by 12th-order pseudo-implicit staggered-grid FD modelling without ABCs and with hybrid ABCs for an elastic model with high V_p/V_s. The velocity and density parameters of the model are from the paper by Opršal and Zahradník (1999). Figures (b)–(f) include 2 panels with *x*- and *z*-components from left to right. Wavefields of 10 grids are used for ABCs and not shown in figures (d) and (f).

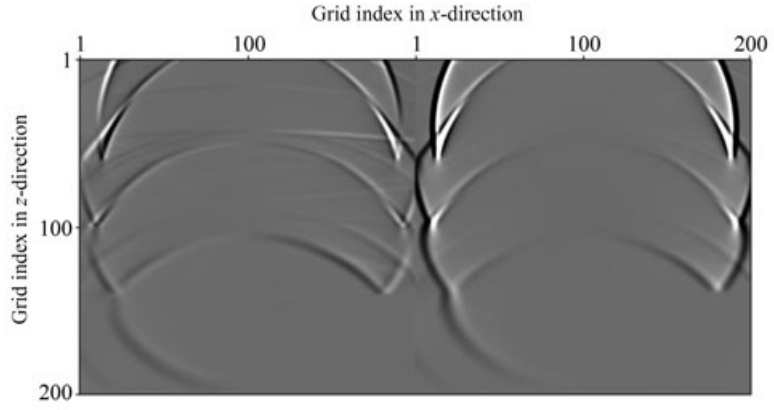

(d) Snapshot at 2000 ms with hybrid ABCs ($N = 10$)

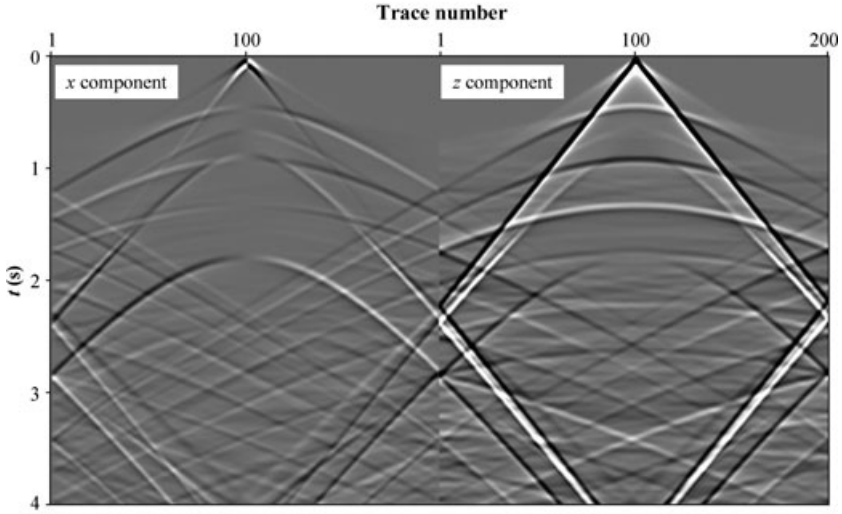

(e) Seismogramsms without ABCs

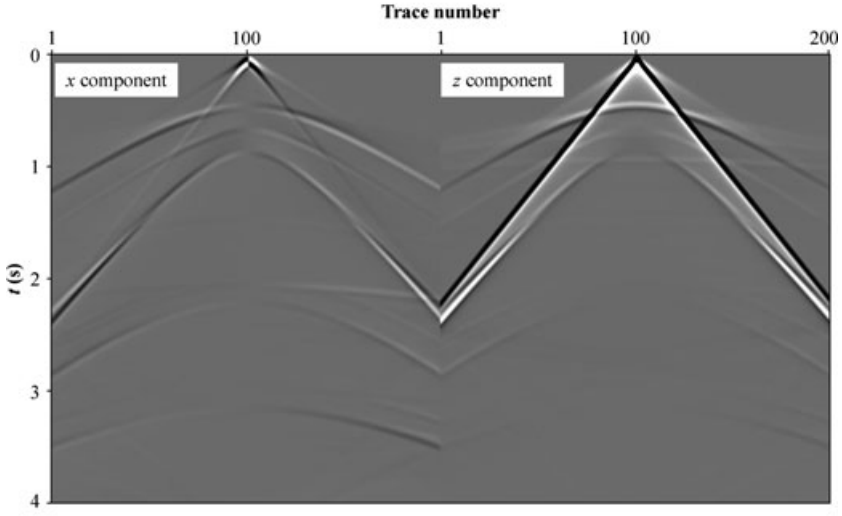

(f) Seismogramsms without hybrid ABCs ($N = 10$)

Figure 7. continued.

and the results show that boundary reflections reduce with an increase of the thickness of the boundary layer but they are still large compared with reflections from strata interfaces since these OWWEs are first-order accuracy. The second-order OWWEs (e.g., Clayton and Engquist 1977) improve the effects of absorption. Higher order OWWEs can improve effects of absorption further but are less robust than second-order OWWEs (Higdon 1991). We adopt the second-order OWWEs developed by Higdon (1991). For example, OWWEs for the left boundary are

$$\left(\beta_1\frac{\partial}{\partial t}-v_{\mathrm{p}}\frac{\partial}{\partial x}\right)\left(\beta_2\frac{\partial}{\partial t}-v_{\mathrm{p}}\frac{\partial}{\partial x}\right)u_x=0, \tag{9a}$$

$$\left(\beta_1\frac{\partial}{\partial t}-v_{\mathrm{p}}\frac{\partial}{\partial x}\right)\left(\beta_2\frac{\partial}{\partial t}-v_{\mathrm{p}}\frac{\partial}{\partial x}\right)u_z=0, \tag{9b}$$

where, $\beta_1=1$, $\beta_2=v_{\mathrm{p}}/v_{\mathrm{s}}$ and v_{p} and v_{s} are P- and S-wave velocities respectively. These equations have greater accuracy and better stability than second-order Clayton-Engquist OWWEs (Higdon 1991). We examine second-order Clayton-Engquist OWWEs for hybrid ABCs and the results show poor stability.

The wavefield values at the left boundary can be approximately predicted by the following formulas (Higdon 1991)

$$u_{x(0,j,k+1)}=\sum_{i=1}^{2}\gamma_{0,i}u_{x(i,j,k+1)}+\sum_{l=0}^{1}\sum_{i=0}^{2}\gamma_{1+l,i}u_{x(i,j,k-l)}, \tag{10a}$$

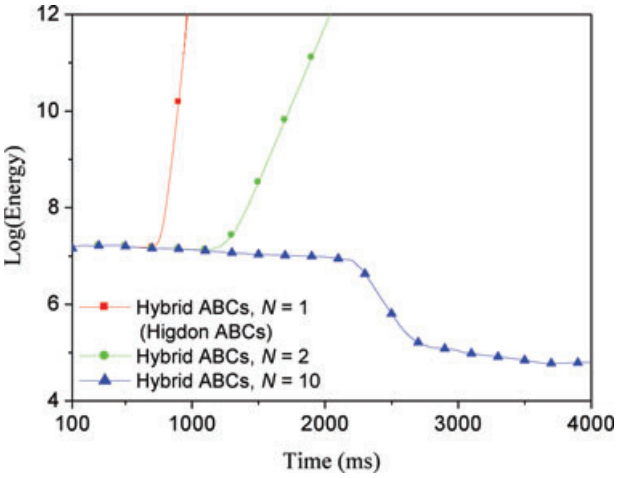

Figure 8. Variation of energy in the inner area with the modelling recursion time for the elastic model with high $V_{\mathrm{p}}/V_{\mathrm{s}}$ shown in Fig. 7. All the modelling parameters are the same as those used in Fig. 7 except that the inner area is fixed as 995 m × 995 m.

$$u_{z(0,j,k+1)}=\sum_{i=1}^{2}\gamma_{0,i}u_{z(i,j,k+1)}+\sum_{l=0}^{1}\sum_{i=0}^{2}\gamma_{1+l,i}u_{z(i,j,k-l)}, \tag{10b}$$

where $(i,\ j,\ k)$ represents $(ih,\ jh,\ k\tau)$ and $\gamma_{i,j}$ can be calculated from the following equation by comparing the coefficients of $x^j y^i$ (Higdon 1991)

$$\begin{aligned}&-1+\gamma_{0,1}x+\gamma_{1,0}y+\gamma_{0,2}x^2+\gamma_{2,0}y^2\\&\quad+\gamma_{1,1}xy+\gamma_{1,2}x^2y+\gamma_{2,1}xy^2+\gamma_{2,2}x^2y^2=\\&\quad-(1+q_{1,1}x+q_{1,2}y+q_{1,3}xy)(1+q_{2,1}x+q_{2,2}y+q_{2,3}xy),\end{aligned} \tag{11}$$

where,

$$q_{i,1}=\frac{b(\beta_i+r)-r}{(\beta_i+r)(1-b)},\quad q_{i,2}=\frac{b(\beta_i+r)-\beta_i}{(\beta_i+r)(1-b)},$$
$$q_{i,3}=\frac{b}{b-1},(i=1,2); \tag{12a}$$

$$r=\frac{v_{\mathrm{p}}\tau}{h}; \tag{12b}$$

b is a constant usually ranging from 0.3–0.5 (Higdon 1991), h is grid size and τ is time step.

At a corner of a rectangular domain, we calculate the displacements by applying the boundary condition on both of the intersecting boundary segments right up to the corner. For instance, u_{x} of the top-left corner is predicted by

$$\begin{aligned}u_{x(0,0,k+1)}=&\sum_{i=1}^{2}0.5\gamma_{0,i}\left(u_{x(i,0,k+1)}+u_{x(0,i,k+1)}\right)\\&+\sum_{l=0}^{1}\sum_{i=0}^{2}0.5\gamma_{1+l,i}\left(u_{x(i,0,k-l)}+u_{x(0,i,k-l)}\right).\end{aligned} \tag{13}$$

u_{z} of the top-left corner can be predicted by a similar equation.

HYBRID ABSORPTION BOUNDARY CONDITIONS

Suggested by the hybrid ABCs used in standard grids (Liu and Sen, 2010a), for staggered grids, we still divide the computational domain into the boundary (Area III: B_1), transition (Area II: B_2, B_3, . . ., B_N; D_1, D_2, . . ., D_N) and inner (Area I) areas shown in Fig. 1. The procedure used to calculate wavefield values at a given time step is as follows:

(**1**) calculate the wavefield values within Areas I, II and III by the WEs-based formulas (2a) and (2b).

(**2**) calculate the wavefield values at Areas II and III by OWWEs-based prediction formulas such as (10a), (10b) and (13).

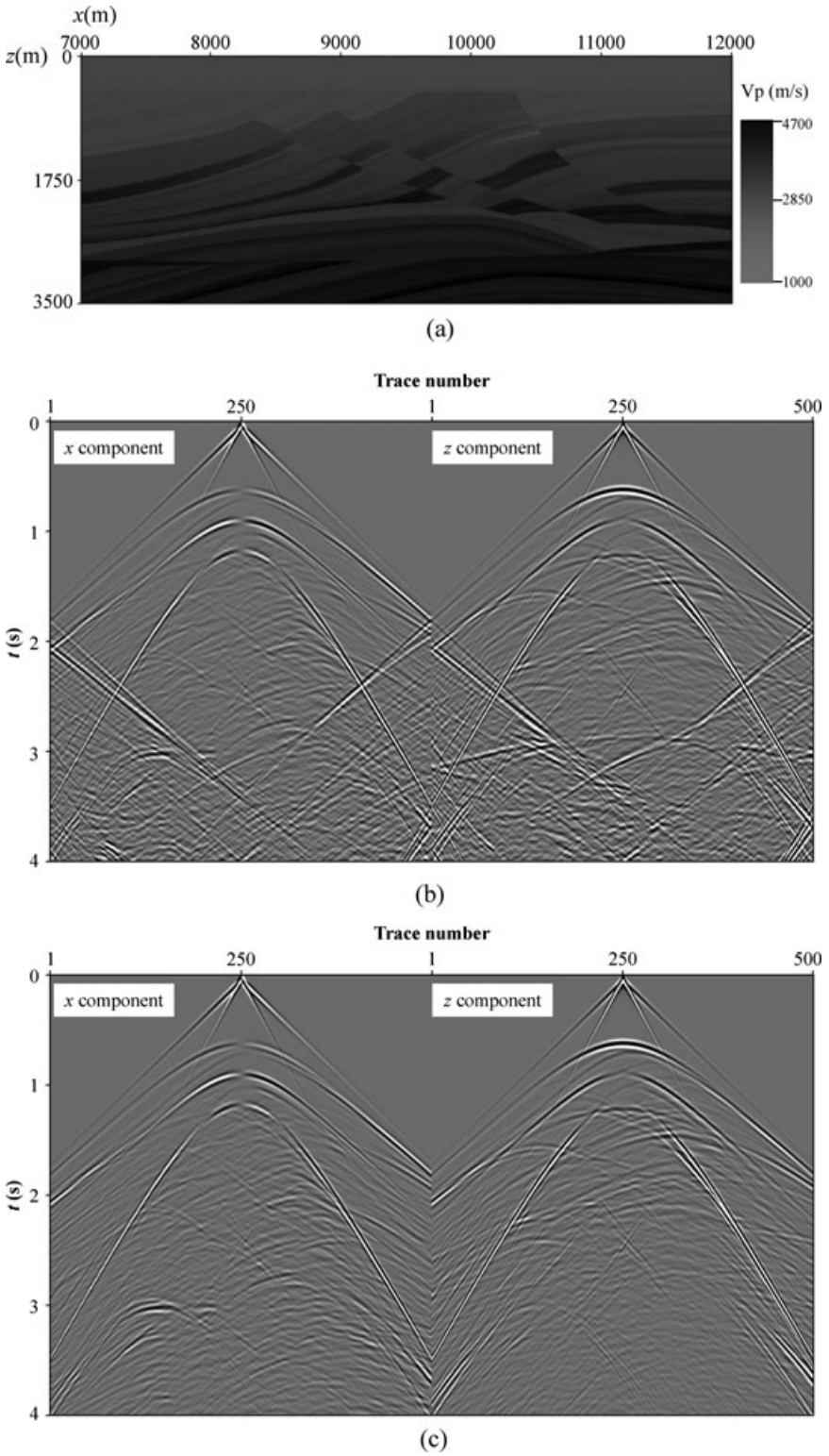

Figure 9. Seismograms computed by 12th-order pseudo-implicit staggered-grid FD modelling for the elastic Marmousi model respectively with non-ABCs and hybrid ABCs ($N = 10$). Figures (b) and (c) include 2 panels with x- and z-components from left to right. Wavefields of 10 grids are used for ABCs and not shown in figure (c).

(3) linearly weigh the values of each grid within Areas II and III from steps (1) and (2) to obtain the final wavefield values for these grids, which is, $u_{x,\mathrm{B}_i} = w_{\mathrm{B}_i} u^{(1)}_{x,\mathrm{B}_i} + (1 - w_{\mathrm{B}_i}) u^{(2)}_{x,\mathrm{B}_i}$ and $u_{z,\mathrm{D}_i} = w_{\mathrm{D}_i} u^{(1)}_{z,\mathrm{D}_i} + (1 - w_{\mathrm{D}_i}) u^{(2)}_{z,\mathrm{D}_i}$ $(i = 1, 2, ..., N)$, where, u_{x,B_i} and u_{z,D_i} are the final wavefield values of the x- and z-component displacements respectively on B_i. D_i, $u^{(1)}_{x,\mathrm{B}_i}$ and $u^{(1)}_{z,\mathrm{D}_i}$ are the wavefield values of the x- and z-component displacements respectively on B_i and D_i determined by step (1), $u^{(2)}_{x,\mathrm{B}_i}$ and $u^{(2)}_{z,\mathrm{D}_i}$ are determined by step (2) and w_{B_i} and w_{D_i} are weight coefficients. Note that the weight coefficients w_{B_i} and w_{D_i} are different. Here, we use linear weight coefficients that generally generate better absorptions than some other non-linear weight coefficients, then, $w_{\mathrm{B}_i} = (i - 1)/N$ and $w_{\mathrm{D}_i} = (i - 0.5)/N$ $(i = 1, 2, ..., N)$.

EXAMPLES

Explicit finite difference, pseudo-implicit FD and pseudo-spectral modelling for a homogeneous model

To examine the effectiveness of the hybrid ABCs for elastic staggered-grid modelling, we perform numerical modelling of 2D elastic wave equations on staggered grids by explicit FD, pseudo-implicit FD and pseudo-spectral methods for a homogeneous model. Note that all modelling schemes are explicit in the time-domain.

Figure 2 shows snapshots computed by explicit staggered-grid FD modelling for a 2D homogeneous elastic model with hybrid ABCs. Each figure includes two panels with x- and z-components from left to right. The model's P-wave velocity, S-wave velocity and density are 3000 m/s, 1500 m/s and 2100 kg/m^3 respectively, grid size is 10 m × 10 m, grid dimensions are 201 × 201 for u_x and 200 × 200 for u_z and the time step is 1 ms. 20th- and 2nd-order finite differences are used respectively for spatial and temporal discretizations. A source pulse of 20 Hz sine function with one period length, located at the centre of the model, is added into the z-component displacement to generate vibration. The free surface condition is not included here. From Fig. 2, we can see that the Higdon ABCs absorb much of the incident wave energy but boundary reflections can still be seen in Fig. 2(a). Figure 2(a–c) demonstrates that the boundary reflections decrease with the increase of the absorbing area width N for the hybrid ABCs. Significant absorption is obtained when $N = 10$. These conclusions can also be drawn from Fig. 3, which shows the direct and the residual edge reflected waves resulting from the Higdon and hybrid ABCs. Note that the Higdon ABCs make the modelling unstable for modelling a long time series, for example, the modelling becomes unstable for this homogeneous model when $t > 800$ ms and the stability of the modelling is greatly improved with the increase of N, which can be proved by Fig. 4.

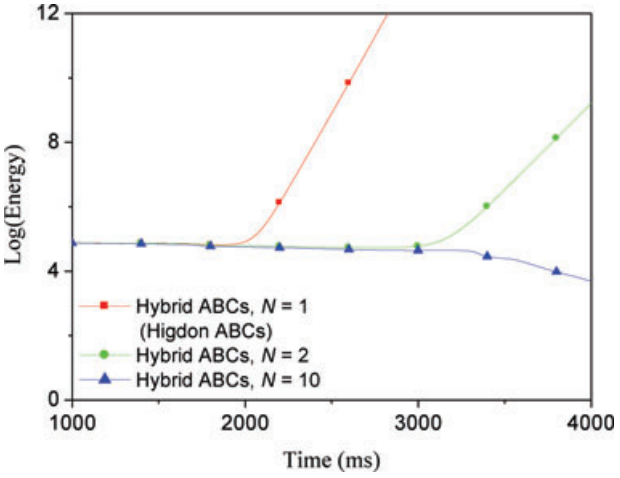

Figure 10. Variation of energy in the inner area with the modelling recursion time for the Marmousi model shown in Fig. 9. All the modelling parameters are the same as those used in Fig. 9. The inner area is fixed as 5000 m × 3500 m.

Figure 5 shows snapshots computed by pseudo-implicit staggered-grid FD modelling for the 2D homogeneous elastic model with hybrid ABCs. The model and simulation parameters are the same as those used in Fig. 3 except for the calculation method of spatial derivations. The modelling with the Higdon ABCs ($N = 1$) becomes unstable for this homogeneous model when $t > 800$ ms. Note that a 12th-order pseudo-implicit FD has nearly the same accuracy as a 22nd-order explicit FD but it requires less computation time (Liu and Sen 2009). Figure 5 suggests that these hybrid ABCs work well for pseudo-implicit FD modelling.

For the pseudo-spectral modelling, our modelling tests suggest that the pseudo-spectral modelling with the Higdon ABCs ($N = 1$) is unstable. The stability of the modelling is improved with the increase of N and the modelling is highly stable and yields great absorption when $N = 10$. Figure 6 shows snapshots computed by staggered-grid pseudo-spectral modelling for the 2D homogeneous elastic model with hybrid *ABCs*. This figure can be compared with Fig. 5.

An elastic model with high V_p/V_s

Opršal and Zahradník (1999) reported that when one model has high V_p/V_s, the stability is critical for the P-SV formulae combined with ABCs. To test the stability of the proposed

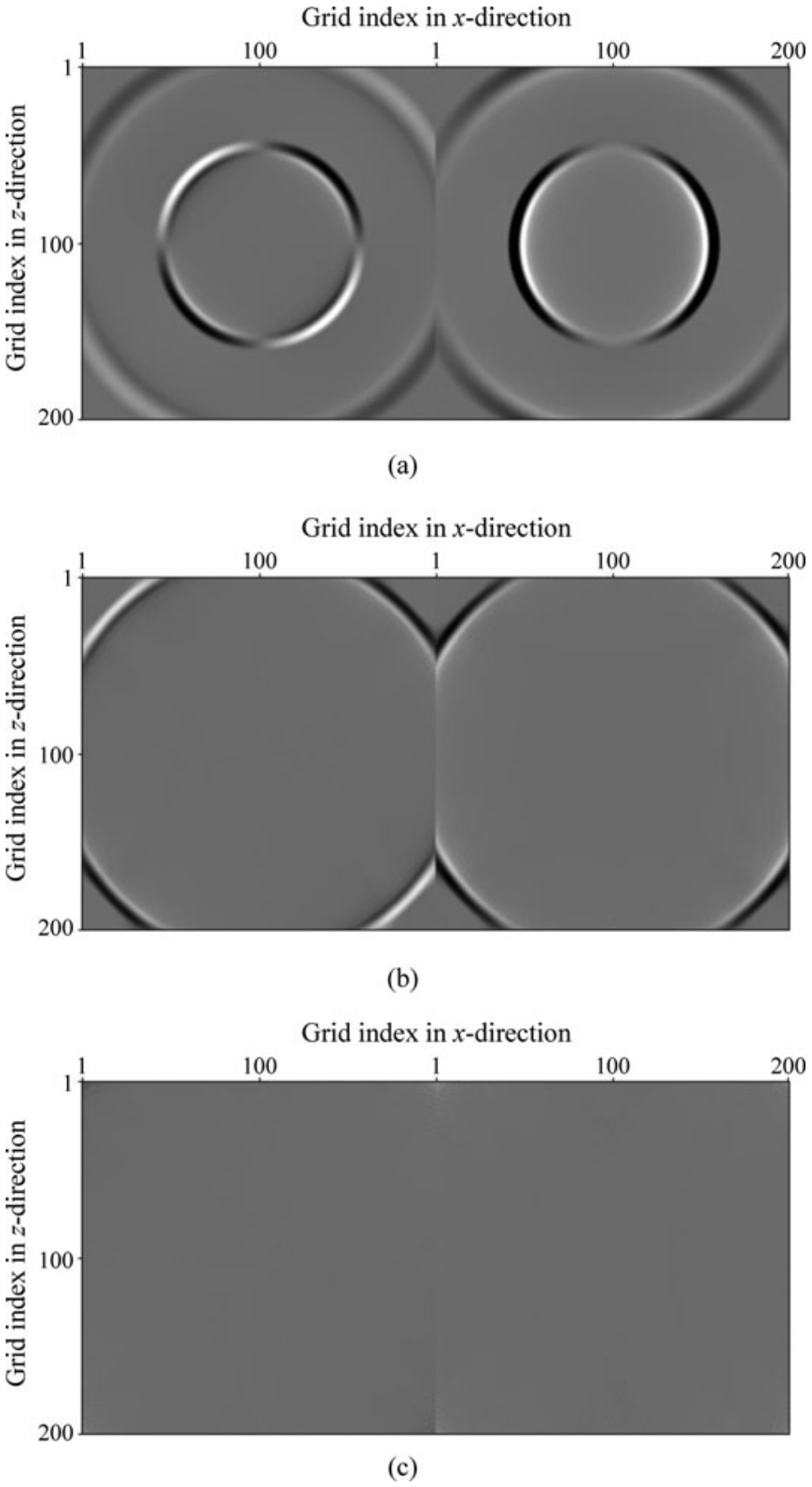

Figure 11. Snapshots computed by 20th-order explicit rotated staggered-grid FD modelling for the 2D homogeneous elastic model with hybrid ABCs ($N = 10$). (a) $t =$ 400 ms, (b) $t = 800$ ms, (c) $t = 1000$ ms. Each figure includes 2 panels with x- and z-components from left to right. The model and modelling parameters are the same as those used in Fig. 2.

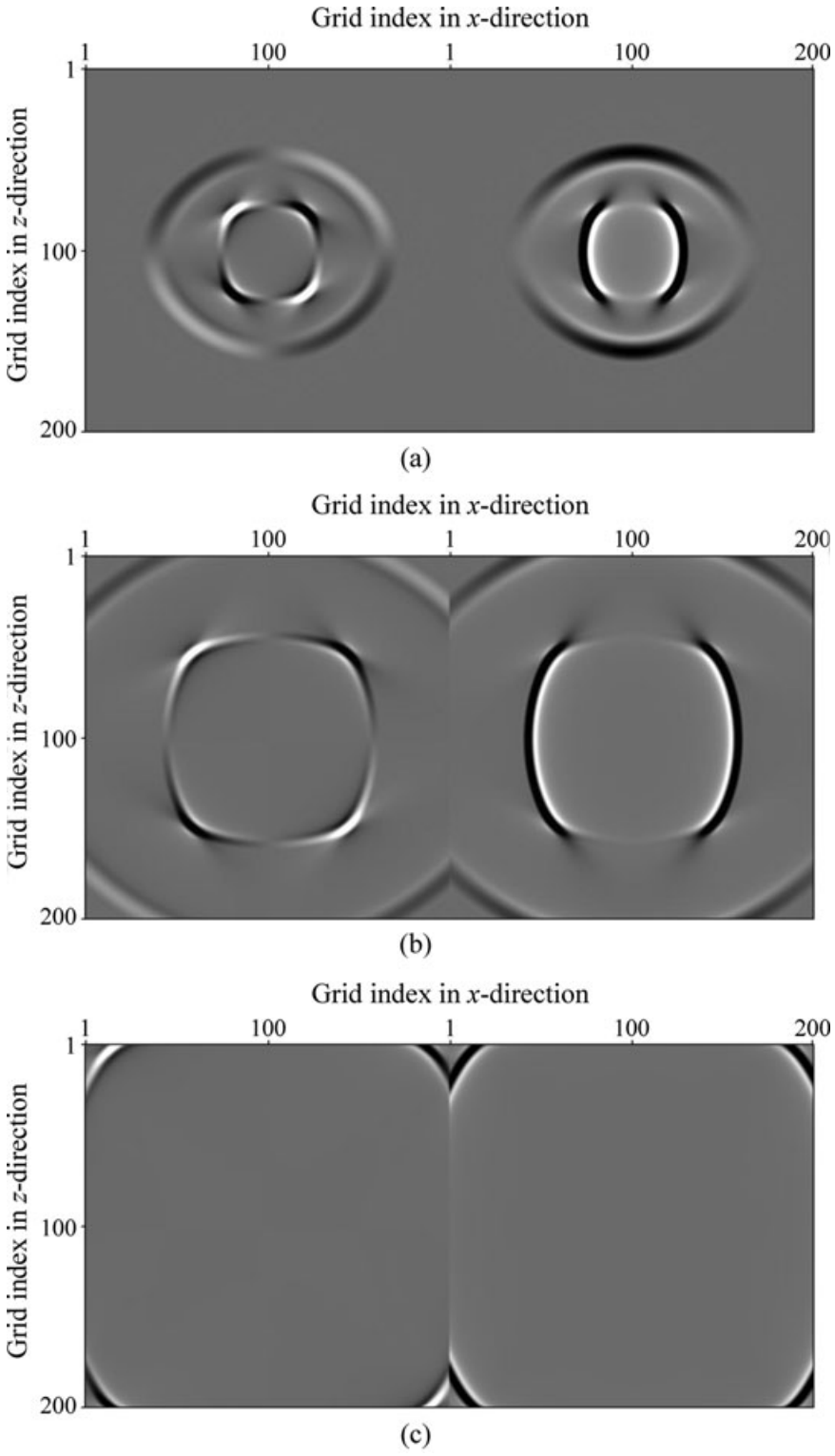

Figure 12. Snapshots computed by 20th-order explicit staggered-grid FD modelling for the 2D homogeneous VTI elastic model with hybrid ABCs ($N = 10$). (a) $t = 200$ ms, (b) $t = 400$ ms, (c) $t = 800$ ms, (d) $t = 1000$ ms. Each figure includes 2 panels with x- and z-components from left to right.

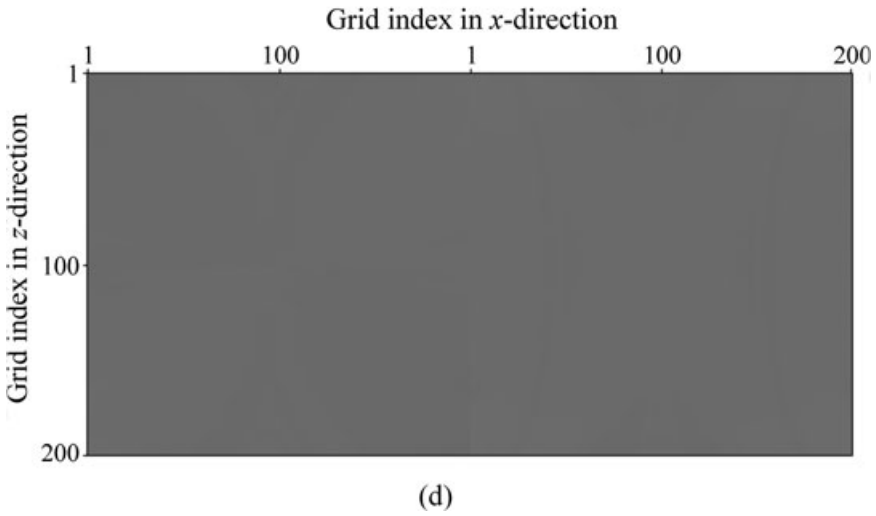

Figure 12. continued.

scheme of elastic staggered-grid modelling with hybrid ABCs, we design a model with high V_p/V_s as shown in Fig. 7(a). The velocity and density parameters of the model are from the paper by Opršal and Zahradník (1999). The grid size is 5 m × 5 m, grid dimensions are 201 × 201 for u_x and 200 × 200 for u_z and the time step is 0.5 ms. Since pseudo-spectral modelling requires the most computation time and pseudo-implicit FD takes less computation time than explicit FD for the same high-order modelling accuracy, we adopt pseudo-implicit FD to perform the following modelling. 12th-order pseudo-implicit and 2nd-order explicit finite differences are used for spatial and temporal discretizations, respectively. A source pulse of 10 Hz sine function with one period length is added into the *x*-component to generate vibration. The receivers for u_x are located at $z = 200$ m and for u_z at $z = 202.5$ m. The free surface condition is not included here. Figure 7(b–f) shows snapshots and seismograms without ABCs and with hybrid ABCs ($N = 10$). From this figure, it follows that the modelling with the hybrid ABCs ($N = 10$) is stable and significantly absorbs boundary reflections.

To demonstrate the stability of the proposed scheme further, variation of energy in the inner area with the modelling recursion time for different absorption thickness N of ABCs is calculated and shown in Fig. 8. From this figure, one can see that

- the modelling with the Higdon ABCs ($N = 1$) becomes unstable when the recursion time is approximately greater than 650 ms.
- the stability is significantly improved with the increase of N.
- the modelling with the hybrid ABCs ($N = 10$) is still stable when the recursion time is equal to 4000 ms.

The Marmousi elastic model

Last, we perform modelling on the Marmousi elastic model to demonstrate the validity of the proposed scheme for complicated elastic models with lateral variations.

Figure 9 shows seismograms computed by implicit staggered-grid FD modelling for the Marmousi model with non-ABCs and hybrid ABCs. The grid size is 10 m × 10 m, grid dimensions are 501 × 351 for u_x and 500 × 350 for u_z and the time step is 1 ms. 12th-order implicit and 2nd-order explicit finite differences are used for spatial and temporal discretizations, respectively. A source pulse of 15 Hz sine function with one period length, located at the grid point (2500 m, 10 m), is added into the *x*-component to generate vibration. The receivers for u_x are located at $z = 10$ m and for u_z at $z = 5$ m. The free surface condition is included here and we only let u_x of the surface be zero to avoid generating Rayleigh waves. From this figure, it follows that the hybrid ABCs significantly absorb boundary reflections and work well for a complicated velocity model. Figure 10 shows a variation of energy in the inner area with the modelling recursion time for different N, which also demonstrates that the modelling with the Higdon ABCs ($N = 1$) becomes unstable when $t > 2000$ ms and the

hybrid ABCs ($N = 10$) lead to greatly improve the modelling stability.

DISCUSSION

In this section, we extend the hybrid absorbing boundary conditions to rotated staggered-grid modelling in isotropic medium, staggered-grid modelling in vertically transversely isotropic medium and rotated staggered-grid modelling in tilted transversely isotropic medium.

Hybrid ABCs for elastic rotated staggered-grid modelling

We combine elastic rotated staggered-grid modelling (Saenger, Gold and Shapiro 2000) with the hybrid ABCs to test their validity. Unlike conventional staggered-grid discretization shown in Fig. 1, u_x and u_z are on the same grids under rotated staggered-grid discretization. Therefore, we can use the hybrid ABCs given in the paper by Liu and Sen (2010a) except OWWEs. Wavefield values at the boundaries and corners are predicted by Higdon OWWEs as stated in the previous section. To show how the hybrid ABCs work for elastic rotated staggered-grid modelling, we perform modelling on the homogeneous elastic model. Figure 11 shows snapshots computed by 20th-order explicit rotated staggered-grid FD modelling for the 2D homogeneous elastic model with the hybrid ABCs ($N = 10$). One can see significant absorption for boundary reflections. Our modelling also shows that the modelling with the Higdon ABCs ($N = 1$) becomes unstable for this model when $t > 600$ ms. Modelling results demonstrate that the hybrid ABCs work for elastic rotated staggered-grid modelling.

Hybrid ABCs for VTI elastic staggered-grid modelling

In 2D VTI elastic media, the displacement-stress relations of wave equations are described by equations (1a) and (1b) and the following three equations (Carcione 1995)

$$\tau_{xx} = c_{11}\frac{\partial u_x}{\partial x} + c_{13}\frac{\partial u_z}{\partial z}, \tag{14a}$$

$$\tau_{zz} = c_{13}\frac{\partial u_x}{\partial x} + c_{33}\frac{\partial u_z}{\partial z}, \tag{14b}$$

$$\tau_{xz} = c_{44}\left(\frac{\partial u_z}{\partial x} + \frac{\partial u_x}{\partial z}\right), \tag{14c}$$

where c_{11}, c_{13}, c_{33} and c_{44} are elastic moduli.

The explicit FD modelling method is used to numerically solve wave equations (1a), (1b), (14a), (14b) and (14c) on staggered grids (Carcione 1999). The Higdon OWWEs (9a) and (9b) are used for the hybrid ABCs. Note that in these OWWEs, $\beta_1 = 1$ and $\beta_2 = v_p/v_s$; v_p and v_s are dependent on wave propagation directions. For the top and bottom boundaries, v_p and v_s are equal to vertical velocities, i.e., $v_p = \sqrt{c_{33}/\rho}$ and $v_s = \sqrt{c_{44}/\rho}$. For the left and right boundaries, v_p and v_s are equal to horizontal velocities, i.e., $v_p = \sqrt{c_{11}/\rho}$ and $v_s = \sqrt{c_{44}/\rho}$.

To test the effects of VTI elastic explicit staggered-grid FD modelling with the hybrid ABCs, we perform modelling on the homogeneous VTI elastic model and the modelling snapshots are shown in Fig. 12. The Thomsen anisotropic parameters (Thomsen 1986) of the model are: $v_{p0} = 3000$ m/s, $v_{s0} = 1500$ m/s, $\varepsilon = 0.2$, $\delta = 0.05$, $\gamma = 0.1$. Gridding and other modelling parameters are the same as those used in Fig. 2. From Fig. 12, it follows that the hybrid ABCs can effectively absorb boundary reflections in VTI elastic staggered-grid modelling. The modelling results also show that the modelling with the Higdon ABCs ($N = 1$) becomes unstable for this model when $t > 600$ ms. In addition, we perform pseudo-implicit FD and pseudo-spectral modelling with the hybrid ABCs on the homogeneous VTI elastic model and obtain similar results.

Hybrid ABCs for TTI elastic rotated staggered-grid modelling

In 2D TTI elastic media, the displacement-stress relations of wave equations are described by equations (1a) and (1b) and the following equations (e.g., Winterstein 1990; Liu, Li and Mou 1998)

$$\rho\frac{\partial^2 u_y}{\partial t^2} = \frac{\partial \tau_{yx}}{\partial x} + \frac{\partial \tau_{yz}}{\partial z}, \tag{15a}$$

$$(\tau_{xx}, 0, \tau_{zz}, \tau_{yz}, \tau_{zx}, \tau_{xy})^{\mathrm{T}} = \boldsymbol{D}\left(\frac{\partial u_x}{\partial x}, 0, \frac{\partial u_z}{\partial z}, \frac{\partial u_y}{\partial z}, \frac{\partial u_x}{\partial z} + \frac{\partial u_z}{\partial x}, \frac{\partial u_y}{\partial x}\right)^{\mathrm{T}}, \tag{15b}$$

where, $\boldsymbol{D} = [d_{ij}]_{6\times 6}$ is the elastic modulus matrix in an observed coordinate system and can be determined by $\boldsymbol{D} = \boldsymbol{M}\boldsymbol{C}\boldsymbol{M}^{\mathrm{T}}$, here, $\boldsymbol{C} = [c_{ij}]_{6\times 6}$ is the elastic modulus matrix in a natural coordinate system, $\boldsymbol{M}$ is the Band transformation matrix (Winterstein, 1990) and T represents a matrix transpose.

The rotated staggered-grid FD modelling method is used to numerically solve wave equations (1a), (1b), (15a) and (15b). The hybrid ABCs adopt the Higdon OWWEs (9a) and (9b)

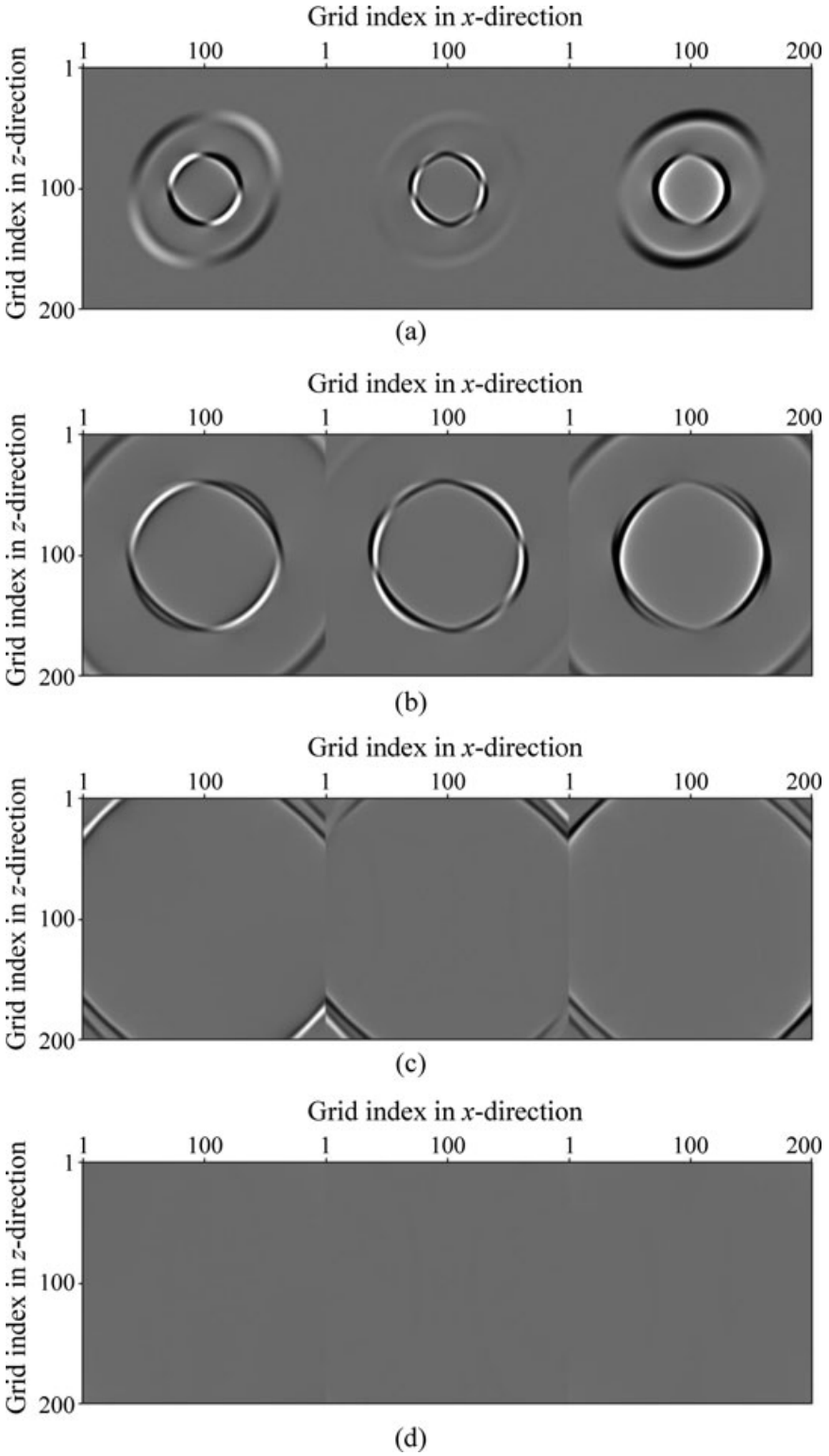

Figure 13. Snapshots computed by 40th-order explicit rotated staggered-grid FD modelling for the 2D homogeneous TTI elastic model with hybrid ABCs ($N = 10$). (a) $t = 200$ ms, (b) $t = 400$ ms, (c) $t = 800$ ms, (d) $t = 1000$ ms. Each figure includes 3 panels with x-, y- and z-components from left to right.

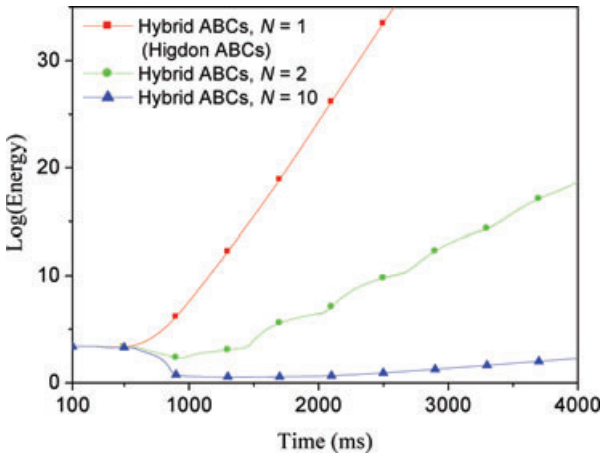

Figure 14. Variation of energy in the inner area with the modelling recursion time for the 2D homogeneous TTI model used in Fig. 13. All the modelling parameters are the same as those used in Fig. 13.

and the following equation

$$\left(\beta_1 \frac{\partial}{\partial t} - v_p \frac{\partial}{\partial x}\right)\left(\beta_2 \frac{\partial}{\partial t} - v_p \frac{\partial}{\partial x}\right) u_y = 0. \tag{16}$$

For the hybrid ABCs of modelling, v_p and v_s are set as velocities of incident waves normal to boundaries. These velocities can be pre-calculated. Note that usually two different shear-wave velocities exist in TTI medium, we adopt the larger one for v_s.

Figure 13 shows modelling snapshots for a homogeneous TTI elastic model. All the model and simulating parameters are the same as those used in Fig. 12 except that the TTI symmetric axis intersects the horizontal plane at a 30 degree angle, the TTI strike intersects the x-axis at a 45 degree angle and 40th-order rotated staggered FD is used.

From Fig. 13 it can be observed that the hybrid ABCs effectively absorb boundary reflections of three kinds of waves although only two kinds of wave velocities are used for the hybrid ABCs. Another potential way to further improve absorption effects for boundary reflections in TTI medium is to adopt third-order OWWEs (Higdon, 1991) in which three kinds of waves velocities can be involved.

Figure 14 shows energy variation in the inner area with the modelling recursion time for the 2D homogeneous TTI model used in Fig. 13. It can be seen that the Higdon ABCs with $N = 1$ become unstable when $t > 500$ ms and the hybrid ABCs with $N = 10$ greatly improve the modelling stability and are stable when all the waves propagate to boundaries ($t < 1000$ ms) but begin to become unstable when $t > 2000$ ms. Perhaps a potential way to further overcome stability problems is to try the strategy of using damping terms in OWWEs (Mulder 1997).

CONCLUSIONS

We have developed hybrid ABCs for elastic wave modelling on staggered grids using explicit FDM, pseudo-implicit FDM and pseudo-spectral methods based on Higdon second-order one-wave wave equations. We also extended hybrid ABCs for rotated staggered-grid modelling in isotropic medium, staggered-grid modelling in VTI medium and rotated staggered-grid modelling in TTI medium. The modelling examples demonstrate that the hybrid ABCs significantly absorb boundary reflections.

ACKNOWLEDGEMENTS

We thank the editor Dr Tijmen Jan Moser, the associate editor Dr Leo Eisner, reviewer Dr Ivo Oprsal and three anonymous reviewers for constructive criticisms of our paper. This research is supported by the National Nature Science Foundation of China (NSFC) under contract number 41074100 and 40839901 and by the Programme for New Century Excellent Talents in University of Ministry of Education of China under contract number NCET-10-0812.

REFERENCES

Bérenger J.P. 1994. A perfectly matched layer for the absorption of electromagnetic waves. *Journal of Computational Physics* **114**, 185–200.

Carcione J.M. 1995. Constitutive model and wave equations for linear, viscoelastic, anisotropic media. *Geophysics* **60**, 537–548.

Carcione J.M. 1999. Staggered mesh for the anisotropic and viscoelastic wave equation. *Geophysics* **64**, 1863–1866.

Cerjan C., Kosloff D., Kosloff R. and Reshef M. 1985. A nonreflecting boundary condition for discrete acoustic and elastic wave equations. *Geophysics* **50**, 705–708.

Clayton R.W. and Engquist B. 1977. Absorbing boundary conditions for acoustic and elastic wave equations. *Bulletin of the Seismological Society of America* **6**, 1529–1540.

Engquist B. and Majda A. 1977. Absorbing boundary conditions for numerical simulation of waves. *Mathematics of Computation* **31**, 629–651.

Festa G. and Nielsen S. 2003. PML absorbing boundaries. *Bulletin of the Seismological Society of America* **93**, 891–903.

Fornberg B. 1987. The pseudospectral method: Comparisons with finite differences for the elastic wave equation. *Geophysics* **52**, 483–501.

Gao H. and Zhang J. 2008. Implementation of perfectly matched layers in an arbitrary geometrical boundary for elastic wave modeling. *Geophysical Journal International* **174**, 1029–1036.

Heidari A.H. and Guddati M.N. 2006. Highly accurate absorbing boundary conditions for wide-angle wave equations. *Geophysics* **71**, S85–S97.

Higdon R.L. 1991. Absorbing boundary conditions for elastic waves. *Geophysics* **56**, 231–241.

Hu W., Abubakar A. and Habashy T.M. 2007. Application of the nearly perfectly matched layer in acoustic wave modeling. *Geophysics* **72**, SM169–SM175.

Kindelan M., Kamel A. and Sguazzero P. 1990. On the construction and efficiency of staggered numerical differentiators for the wave equation. *Geophysics* **55**, 107–110.

Komatitsch D. and Tromp J. 2003. A perfectly matched layer absorbing boundary condition for the second-order seismic wave equation. *Geophysical Journal International* **154**, 146–153.

Kosloff D. and Baysal E. 1982. Forward modeling by a Fourier method. *Geophysics* **47**, 1402–1412.

Kosloff R. and Kosloff D. 1986. Absorbing boundaries for wave propagation problems. *Journal of Computational Physics* **63**, 363–376.

Liao Z.P., Wong H.L., Yang B.P. and Yuan Y.F. 1984. A transmitting boundary for transient wave analysis. *Scientia Sinica Series A* **27**, 1063–1076.

Liu Y., Li C. and Mou Y. 1998. Elastic wave in transverse isotropic media with dipping symmetric axis. *Oil Geophysical Prospecting* (abstract in English) **33**, 161–169.

Liu Y. and Sen M.K. 2009. An implicit staggered-grid finite-difference method for seismic modeling. *Geophysical Journal International* **179**, 459–474.

Liu Y. and Sen M.K. 2010a. A hybrid scheme for absorbing edge reflections in numerical modeling of wave propagation. *Geophysics* **75**, A1–A6.

Liu Y. and Sen M.K. 2010b. A hybrid absorbing boundary condition for elastic wave modeling with staggered-grid finite difference. 80th SEG meeting, Denver, Colorado, USA, Expanded Abstracts, 2945–2949.

Luo Y. and Schuster G. 1990. Parsimonious staggered grid finite-differencing of the wave equation. *Geophysical Research Letters* **17**, 155–158.

Mittet R. 2002. Free-surface boundary conditions for elastic staggered-grid modeling schemes. *Geophysics* **67**, 1616–1623.

Mulder W.A. 1997. Experiments with Higdon's absorbing boundary conditions for a number of wave equations. *Computational Geosciences* **1**, 85–108.

Opršal I. and Zahradník J. 1999. From unstable to stable seismic modelling by finite-difference method. *Physics and Chemistry of the Earth, Part A: Solid Earth and Geodesy* **24**, 247–252.

Reynolds A.C. 1978. Boundary conditions for the numerical solution of wave propagation problems. *Geophysics* **43**, 1099–1110.

Saenger E.H., Gold N. and Shapiro S.A. 2000. Modeling the propagation of elastic waves using a modified finite-difference grid. *Wave Motion* **31**, 77–92.

Sarma G.S., Mallick K. and Gadhinglajkar V.R. 1998. Nonreflecting boundary condition in finite-element formulation for an elastic wave equation. *Geophysics* **63**, 1006–16.

Sochacki I., Kubichek R., George J., Fletcher W.R. and Smitson S. 1987. Absorbing boundary conditions and surface waves. *Geophysics* **52**, 60–71.

Stacey R. 1988. Improved transparent boundary formulations for the elastic-wave equation. *Bulletin of the Seismological Society of America* **78**, 2089–2097.

Stacey R. 2003. Stability analysis of finite-difference approximations of elastic wave equations. *Bulletin of the Seismological Society of America* **93**, 1198–1211.

Thomsen L. 1986. Weak elastic anisotropy. *Geophysics* **51**, 1954–1966.

Tian X., Kang I., Kim G.Y. and Zhang H. 2008. An improvement in the absorbing boundary technique for numerical simulation of elastic wave propagation. *Journal of Geophysics and Engineering* **5**, 203–209.

Virieux J. 1986. P-SV wave propagation in heterogeneous media: Velocity stress finite difference method. *Geophysics* **51**, 889–901.

Wang T. and Tang X. 2003. Finite-difference modeling of elastic wave propagation: A nonsplitting perfectly matched layer approach. *Geophysics* **68**, 1749–1755.

Winterstein D.F. 1990. Velocity anisotropy terminology for geophysicists. *Geophysics* **55**, 1070–1088.

Zeng Y., He J. and Liu Q. 2001. The application of the perfectly matched layer in numerical modeling of wave propagation in poroelastic media. *Geophysics* **66**, 1258–1266.

Zhou H. and McMechan G.A. 2000. Rigorous absorbing boundary conditions for 3-D one-way wave extrapolation. *Geophysics* **65**, 638–645.